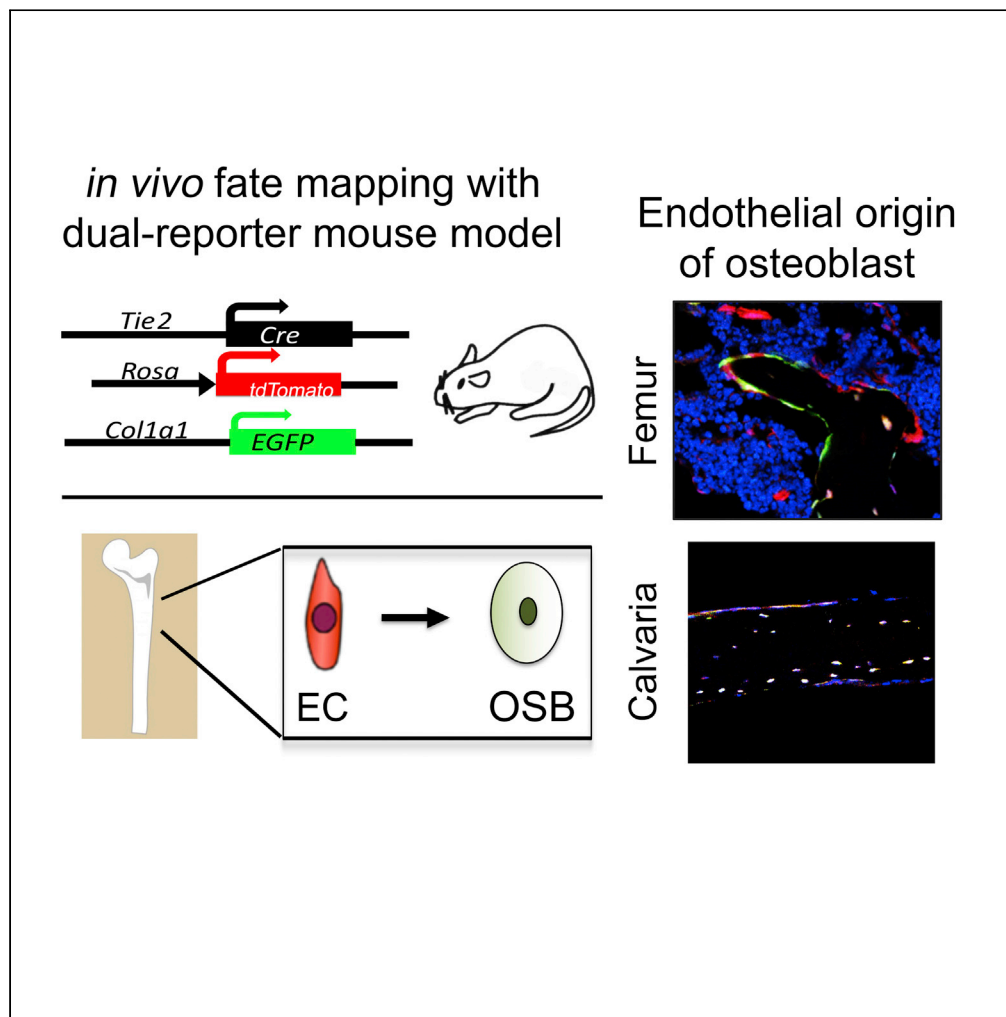


Article

Endothelial-to-osteoblast transition in normal mouse bone development



Song-Chang Lin,
 Guoyu Yu, Yu-
 Chen Lee, ..., Li-
 Yuan Yu-Lee,
 Guocan Wang,
 Sue-Hwa Lin

gwang6@mdanderson.org
 (G.W.)
 slin@mdanderson.org (S.-H.L.)

Highlights

A lineage-tracing mouse model reveals EC-to-OSB transition in normal bone formation

In vivo, cells on bone surface showed both EC (RFP) and OSB (GFP) fluorescence

In vitro, bone marrow- or lung-derived ECs transitioned to OSB and mineralized

RNAseq showed GATA3 transcription factor is involved in EC-to-OSB transition

Lin et al., iScience 26, 105994
 February 17, 2023 © 2023 The Author(s).
<https://doi.org/10.1016/j.isci.2023.105994>

Article

Endothelial-to-osteoblast transition
in normal mouse bone development

Song-Chang Lin,¹ Guoyu Yu,¹ Yu-Chen Lee,¹ Jian H. Song,² Xingzhi Song,³ Jianhua Zhang,³ Theocharis Panaretakis,² Christopher J. Logothetis,² Yoshihiro Komatsu,⁴ Li-Yuan Yu-Lee,⁵ Guocan Wang,^{2,*} and Sue-Hwa Lin^{1,2,6,*}

SUMMARY

Metastatic prostate cancer (PCa) in bone induces bone-forming lesions. We have previously shown that PCa-induced bone originates from endothelial cells (ECs) that have undergone EC-to-osteoblast (OSB) transition. Here, we investigated whether EC-to-OSB transition also occurs during normal bone formation. We developed an EC and OSB dual-color reporter mouse (DRM) model that marks EC-OSB hybrid cells with red and green fluorescent proteins. We observed EC-to-OSB transition (RFP and GFP co-expression) in both endochondral and intramembranous bone formation during embryonic development and in adults. Co-expression was confirmed in cells isolated from DRM. Bone marrow- and lung-derived ECs underwent transition to OSBs and mineralization in osteogenic medium. RNA-sequencing revealed GATA family transcription factors were upregulated in EC-OSB hybrid cells and knockdown of GATA3 inhibited BMP4-induced mineralization. Our findings support that EC-to-OSB transition occurs during normal bone development and suggest a new paradigm regarding the endothelial origin of OSBs.

INTRODUCTION

Prostate cancer (PCa) that has metastasized to bone is an aggressive disease without effective therapies. PCa bone metastasis is frequently associated with osteoblastic bone-forming lesions, indicating crosstalk between metastatic tumor cells and the stromal component.¹ Increases in the expression of bone morphogenetic proteins (BMPs) in tumor cells have been shown to play a role in increased bone formation in metastatic lesions.^{2–5} Such tumor-induced remodeling of the bone microenvironment has been shown to contribute to progression and resistance to bone metastasis therapies.^{6,7}

Although PCa-induced aberrant bone formation was originally thought to result from the expansion of existing osteoblasts (OSBs),¹ Roudier et al.⁸ found that in human PCa bone metastasis, new bone formation was observed in the tumor stroma, not the adjacent bone surface, suggesting an alternative cell source. Indeed, we showed that tumor-associated endothelial cells (ECs) represent one of the cell types that become OSBs through EC-to-OSB transition induced by PCa-secreted BMP4.³ We further elucidated that BMP4 coordinates multiple pathways to reprogram ECs into OSBs.⁹ Using murine EC lines 2H11 and SVR, we showed that BMP4 activates not only the Smad1-Notch-Hey1 pathway to inhibit EC migration and tube formation, but also the GSK3 β - β -catenin-Slug pathway to stimulate the expression of Sp7/Osterix (Osx), a transcription factor that mediates OSB cell fate determination.⁹ These two pathways converge through Smad1-regulated Dlx2 to stimulate osteocalcin expression. Exogenous co-expression of Osx, Dlx2, Slug, and Hey1 is sufficient to trigger EC-to-OSB transition, leading to bone matrix mineralization in the absence of BMP4.⁹

Our previous studies demonstrated that tumor-associated ECs can be reprogrammed to become OSBs. However, it remained unclear whether EC-to-OSB transition occurs in normal bone formation. Thus, in the current study, we examined EC-to-OSB transition during normal bone development using lineage tracing, in which EC-OSB hybrid cells are visualized using both EC and bone lineage markers. We generated dual-color reporter mice (DRM; Col1 α 1-GFP/Tie2-Cre/Rosa-tdTomato), in which ECs express red fluorescent protein (RFP) directed by the Tie2 promoter in Rosa mice, whereas OSBs express green fluorescent

¹Department of Translational Molecular Pathology, The University of Texas MD Anderson Cancer Center, Houston, TX 77030, USA

²Department of Genitourinary Medical Oncology, The University of Texas MD Anderson Cancer Center, Houston, TX 77030, USA

³Department of Genomic Medicine, The University of Texas MD Anderson Cancer Center, Houston, TX 77030, USA

⁴Department of Pediatrics, The University of Texas Medical School at Houston, Houston, TX 77030, USA

⁵Departments of Medicine and Molecular and Cellular Biology, Baylor College of Medicine, Houston, TX 77030, USA

⁶Lead contact

*Correspondence: gwang6@mdanderson.org (G.W.), slin@mdanderson.org (S.-H.L.)

<https://doi.org/10.1016/j.isci.2023.105994>



protein (GFP) driven by the 2.3-kb *Col1 α 1* promoter. The *Tie2* and 2.3-kb *Col1 α 1* promoters were selected to capture EC-to-OSB transition because *Tie2* expression is detected as ECs arise and remains expressed in ECs throughout development,^{10,11} whereas the 2.3-kb *Col1 α 1* promoter is activated in the pre-OSB and OSB stages.¹² In the DRM, EC-OSB hybrid cells are identified as RFP⁺/GFP⁺ dual-positive cells. We found that EC-to-OSB transition occurs in both endochondral and intramembranous bone formation during normal skeletal development, demonstrating that ECs participate in normal bone development. Our findings suggest a new paradigm for EC-to-OSB transition in normal bone development and have important implications for developing strategies for the management of bone-related diseases, including enhancing bone regeneration or inhibiting heterotopic bone formation.

RESULTS

EC-to-OSB transition occurs in early endochondral bone development

To address whether EC-to-OSB transition occurs in normal bone development, we generated DRM (*Col1 α 1*-GFP/*Tie2*-Cre/*Rosa*-tdTomato), in which ECs are marked with tdTomato (RFP) from *Tie2*-Cre/*Rosa*-tdTomato and OSBs are marked with GFP from 2.3-kb *Col1 α 1*-GFP (Figure 1A). *Tie2*, also known as TEK, is expressed during vessel development and plays a role in the formation of blood vessels.¹³ The 2.3-kb α 1(I) collagen promoter is mainly active in the pre-OSB and OSB stages of osteogenesis.^{12,14}

During early development, vascularization begins around embryonic day 8 (E8).^{15,16} Endochondral bone formation occurs around E15, during which blood vessels enter the avascular cartilage and OSBs start to appear,¹⁷ eventually replacing cartilage with bone. The primary ossification center (POC) marks the location in which ossification starts in a developing bone. We found that in DRM, GFP⁺ cells were observed in the femur, tibia, and fibula of E15.5 embryos (Figure 1B), as well as shoulder, rib, forelimb, and hindlimb (Figure S1A). Histological and confocal analysis showed that RFP⁺ cells were abundantly present in the center of the POC in E15.5 femurs (Figure 1C, arrow), consistent with POCs containing a highly branched vessel plexus. Confocal images showed that GFP⁺ cells in the POCs overlapped with RFP⁺ cells in E15.5 femurs (Figure 1C). Although cells in the center of the POC were RFP⁺, cells toward the endosteum gradually gained GFP positivity (Figure 1C, arrowheads). We noted that some cells localized in the endochondral areas showed higher RFP than GFP signals, whereas others showed higher GFP than RFP signals. A different plane of confocal images of E15.5 femurs is shown in Figure S2. *Tie2*⁺ cells, on the expression of Cre, irreversibly express RFP. Therefore, during the entire course of their lifespan, *Tie2*⁺ cells will remain RFP⁺ even if they subsequently lose *Tie2* gene expression. Together, these observations suggest that some of the *Tie2*⁺ cells are undergoing EC (RFP⁺)–to–OSB (GFP⁺) transition during early endochondral bone formation.

EC-to-OSB transition occurs in early intramembranous bone development

Next, we examined whether EC-to-OSB transition also occurs in intramembranous bone formation in the head. In E15.5 DRM, we found that GFP⁺ cells were observed in the calvariae and mandible regions, with the frontal calvariae showing abundant GFP⁺ signals, followed by the parietal calvariae, and the occipital bone showing the least GFP⁺ signals at this developmental stage (Figures 1D and S1B). In frontal calvariae, confocal images showed co-localization of GFP⁺ and RFP⁺ signals in the calvarial OSBs (Figure 1E, arrowheads). These observations suggest that a fraction of *Tie2*⁺ cells are able to become GFP⁺ OSBs, and that EC-to-OSB transition occurs during intramembranous bone formation.

EC-to-OSB transition occurs in adult mouse femurs and calvariae

In the postnatal day 30 (P30) mouse femur, RFP⁺ cells were found to be distributed in the growth plate area and in the bone marrow (Figure 2A). In trabecular bone in the metaphysis, RFP⁺/GFP⁺ dual positivity was found in OSBs present on the bone surface (Figure 2A, top row, arrows) as well as in osteocytes (arrowheads). Among the RFP⁺/GFP⁺ dual-positive cells, some showed higher GFP than RFP signals, whereas others showed higher RFP than GFP signals. Such varied intensity was also observed in the developing E15.5 embryonic bone (Figures 1C and 1E). In the diaphysis area, where trabecular bones were less abundant, RFP⁺/GFP⁺ dual-positive cells were also found on the trabecular bone surface (Figure 2A, bottom row, arrows) and in osteocytes (arrowheads). A similar phenomenon was observed in the tibia (Figure S3A) and lumbar vertebra (Figure S3B). In P30 calvariae, RFP⁺/GFP⁺ dual-positive cells were observed on the surface of calvariae (Figure 2B, arrows) as well as in osteocytes (arrowheads), including at the midline suture region (Figures 2B and S3C). Results similar to those in P30 femurs or calvariae were also observed in femurs

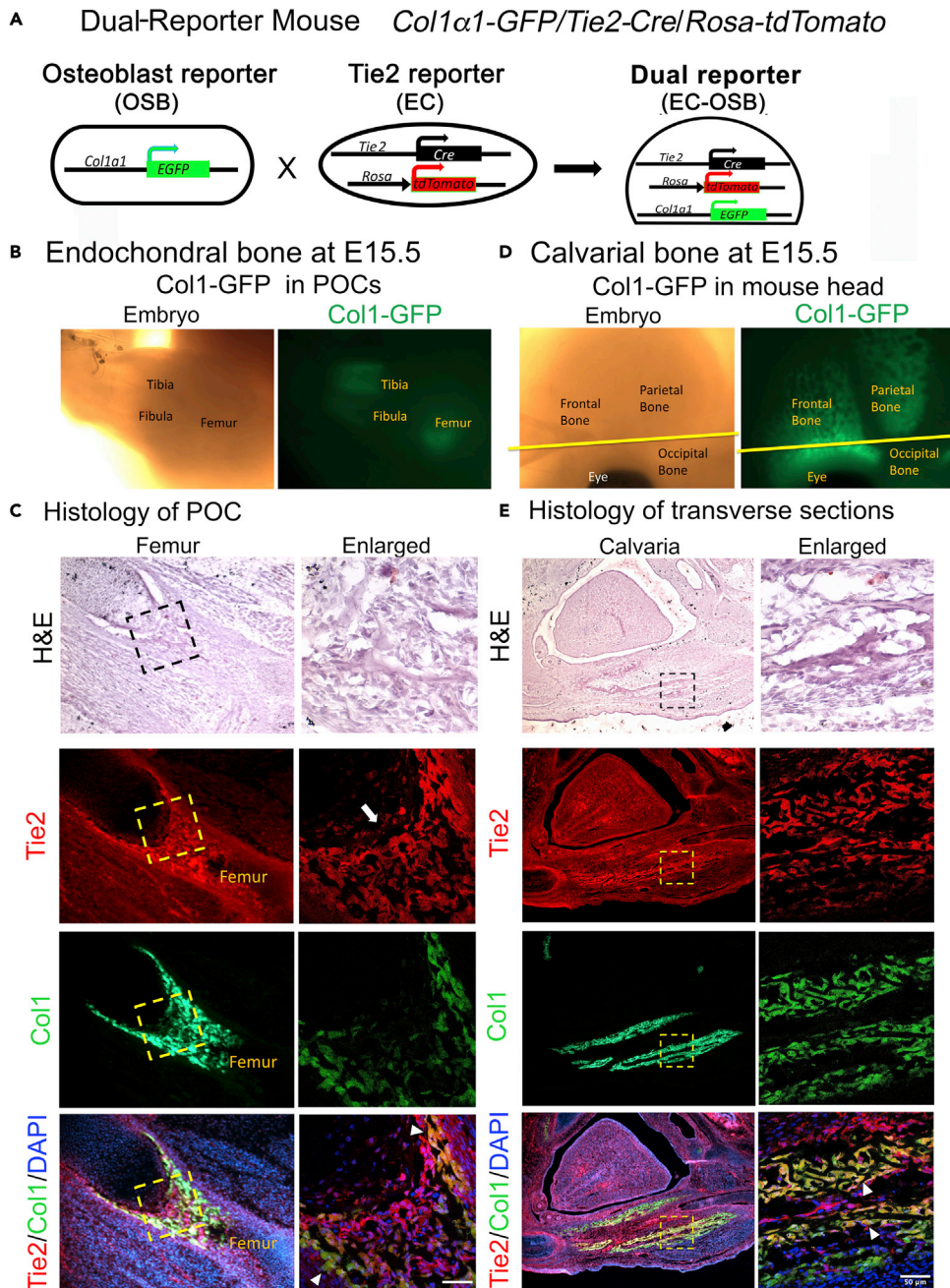


Figure 1. Endothelial-to-osteoblast transition in endochondral and intramembranous bones in embryonic day 15.5 mouse embryo

(A) Breeding scheme of *Col1 α 1-GFP/Tie2-Cre/Rosa-tdTomato* mouse (dual-reporter mouse). The black arrowhead in the *Rosa* gene promoter indicates a *lox-stop-lox* sequence.

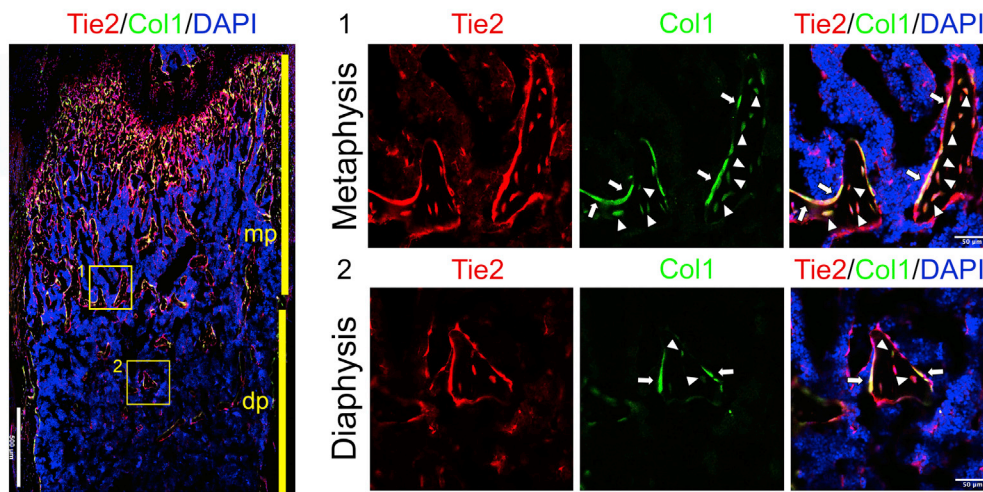
(B) EC-to-OSB transition during endochondral bone formation in DRM. Left, photo of an E15.5 embryo. Right, GFP expression at the POC in mouse femur, tibia, and fibula.

(C) Histology and confocal images of the POC in an E15.5 embryo femur. H&E and expression of RFP (Tie2), GFP (Col1), and merged RFP/GFP/DAPI images. The boxed areas in the left images, enlarged in the right images, show co-localization of RFP⁺ and GFP⁺ cells. Arrow, POC; arrowheads, RFP⁺/GFP⁺ dual-positive cells.

(D) EC-to-OSB transition in calvaria of an E15.5 embryo. Left, photo of an E15.5 embryo head. Right, GFP expression in E15.5 calvarial bone, including the frontal, parietal, and occipital bones. Yellow lines, plane of dissection for (E).

(E) Histology and confocal images of a mouse E15.5 calvaria, analyzed as in (C). The boxed areas in the left images, enlarged in the right images, show RFP⁺/GFP⁺ dual-positive cells (arrowhead). Bars, 50 μ m.

A Co-expression of Tie2 and Col1 in P30 femur



B EC-OSB cells in P30 calvaria

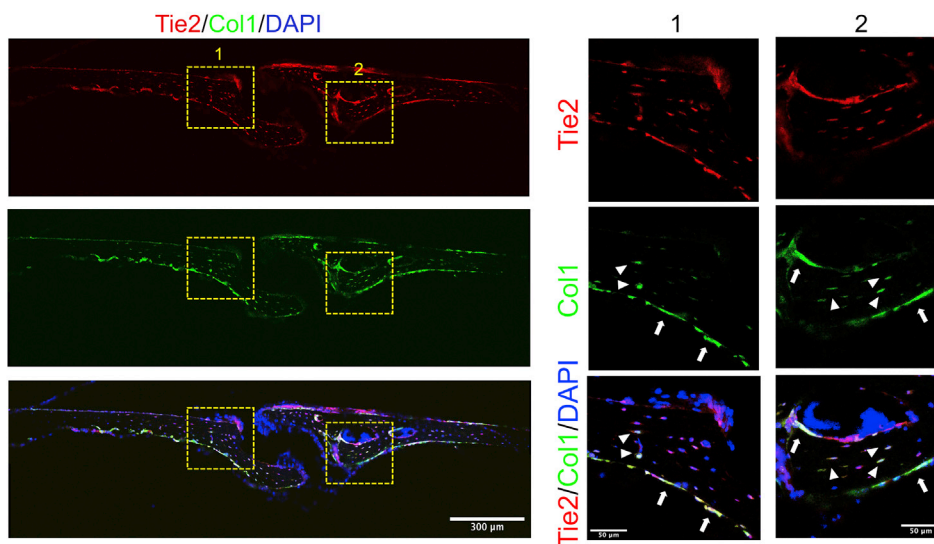


Figure 2. Endothelial-to-osteoblast transition in endochondral and intramembranous bones in postnatal day 30 mouse

(A) Confocal images of growth plate/metaphysis/diaphysis area of a femur from a P30 DRM. The boxed areas at left are enlarged at right. Box 1, metaphysis (mp). Box 2, diaphysis (dp). Arrows, RFP⁺/GFP⁺ dual-positive OSBs on bone surface; arrowheads, dual-positive osteocytes.

(B) Confocal images of intramembranous bone in a postnatal P30 calvaria. Boxes, enlarged areas on each side of the midline suture junction. Arrows and arrowheads as in (A).

and calvariae from 6-month-old DRM (Figure S4). These observations suggest that EC-to-OSB transition occurs during bone formation in both the embryonic and adult stages.

Tie2-RFP and Col1-GFP are co-expressed in the individual cells of dual-reporter mice

To further confirm that Tie2-RFP and Col1-GFP are co-expressed in the same cell, we isolated cells from the bone marrow of DRM. The majority of fluorescence-positive cells in bone marrow samples were RFP⁺, as expected (Figure 3A, upper panels). For the RFP⁺/GFP⁺ dual-positive cells found in the bone marrow, the levels of RFP and GFP in the individual cells varied (Figure 3A, lower panels), as was also the case for the RFP⁺/GFP⁺ dual-positive cells in the femurs (Figure 2A). Although rare, RFP⁺ or RFP⁺/GFP⁺ cells

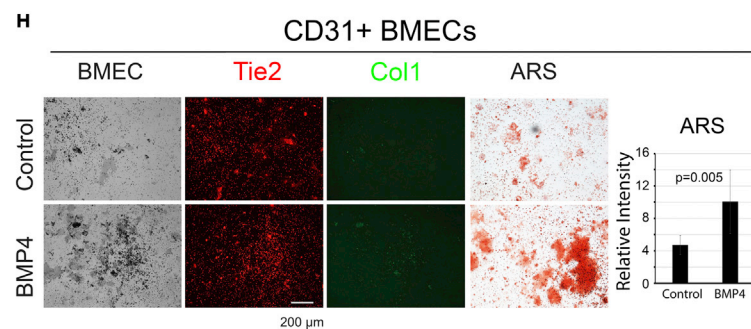
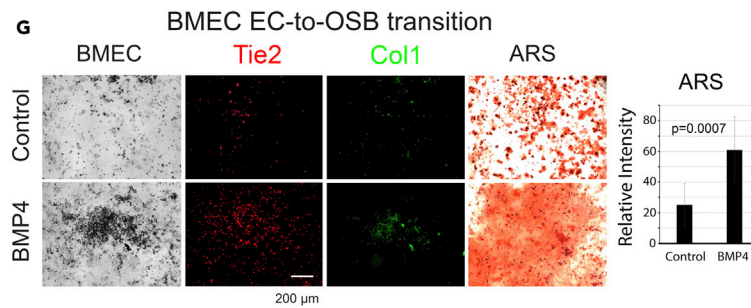
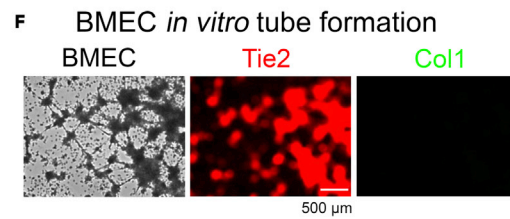
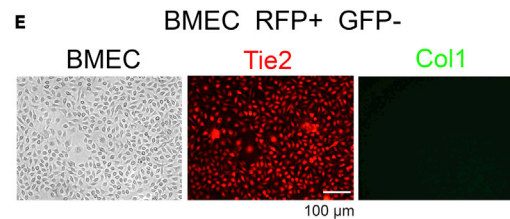
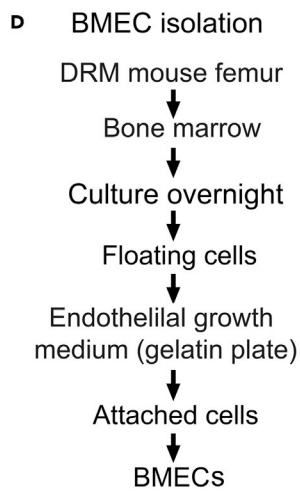
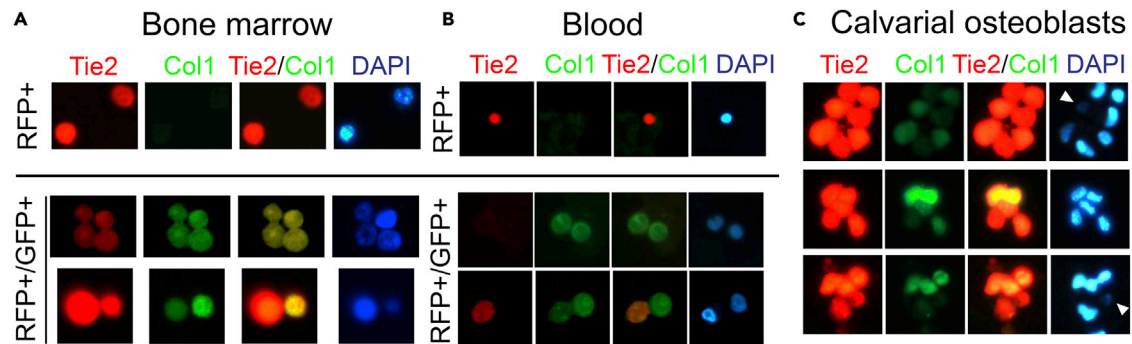


Figure 3. Co-expression of RFP and GFP in individual cells and transition of RFP⁺ bone marrow endothelial cells to RFP⁺/GFP⁺ osteoblasts *in vitro*

(A) Bone marrow cells were isolated from a femur of a 3-month-old DRM mouse. Several cells were selected to show the varying levels of RFP and GFP expression in RFP⁺/GFP⁺ dual-positive cells.
 (B) Blood cells from 3-month-old DRM. Red blood cells were removed by hypotonic disruption in NH₄Cl lysis buffer. Circulating RFP⁺ or RFP⁺/GFP⁺ dual-positive cells were found in blood samples.
 (C) Calvarial OSBs from a 3-month-old DRM were isolated by collagenase digestion. Calvarial OSBs showed RFP⁺/GFP⁺ dual positivity with varying levels of RFP and GFP. Arrowheads, nuclei with faint DAPI signals.
 (D) Procedure for isolating bone marrow endothelial cells (BMECs) from femurs of DRM.
 (E) BMECs were RFP⁺ but GFP⁻.
 (F) BMECs formed a tube structure in an endothelial tube formation assay.
 (G and H) BMECs from (E) were cultured in StemPro osteogenic medium with and without BMP4 (100 ng/mL) for 21 days. BMP4 and media were refreshed twice per week. GFP⁻ cells became GFP⁺ after 21 days. Alizarin Red S (ARS) staining showed mineralized bone nodules in control and BMP4-treated RFP⁺/GFP⁺ BMECs. The staining was quantified using ImageJ software. Data are represented as mean ± SD (H) CD31⁺ cells were isolated from BMECs from (E) with rat anti-mouse CD31 antibody-conjugated Dynabeads. CD31⁺ cells were subjected to *in vitro* osteogenic assays as described in (G). Data are represented as mean ± SD.

were also observed in DRM blood (Figure 3B). The presence of RFP⁺/GFP⁺ OSBs in mouse blood is consistent with previous reports by Eghbali-Fatourehchi et al.¹⁸ and Suriyachand et al.,¹⁹ which showed circulating OSB-lineage cells in human blood samples. In contrast to bone marrow and blood samples, calvarial OSBs isolated by collagenase digestion of DRM calvariae were all RFP⁺/GFP⁺ dual positive with varying degrees of RFP or GFP in the individual cells, as expected (Figure 3C). These observations suggest that Tie2-RFP and Col1-GFP are co-expressed in the same cells from DRM.

RFP⁺ bone marrow endothelial cells can transition to GFP⁺ osteoblasts *in vitro*

To examine whether ECs isolated from the bone marrow of DRM can transition to OSBs *in vitro*, bone marrow cells were flushed out of the femurs and tibias of a 7-week-old DRM. Bone marrow cells were processed as described by Soleimani and Nadri²⁰ (Figure 3D), and the non-adherent cells, which were devoid of bone marrow stromal cells, were collected. To enrich for bone marrow ECs (BMECs), the non-adherent cells were plated onto gelatin-coated plates, then cultured in EC growth medium, both of which are essential for BMEC growth²¹ (Figure 3D). Isolated BMECs were RFP⁺ but GFP⁻, as expected (Figure 3E). To confirm their EC properties, we performed endothelial tube formation assays. BMECs formed vessel networks, a characteristic EC phenotype, when cultured on Matrigel (Figure 3F). The RFP⁺ BMECs (from Figure 3E) were cultured in osteogenic medium with or without BMP4 for 21 days. Under these conditions, RFP⁺ BMECs turned into RFP⁺/GFP⁺ dual-positive cells (Figure 3G). Alizarin Red staining showed that the RFP⁺/GFP⁺ clusters were mineralized bone nodules (Figure 3G). Because the StemPro osteogenic medium contains an unspecified concentration of BMP2, we found that RFP⁺-to-RFP⁺/GFP⁺ transition also occurred without exogenous BMP4 (Figure 3G, Control). However, when medium was diluted 2-fold to reduce the strength of the endogenous supplements, RFP⁺-to-RFP⁺/GFP⁺ transition and mineralization were nevertheless enhanced by the addition of BMP4 (Figure 3G, BMP4). We further isolated CD31⁺ ECs from the Tie2⁺ BMECs using CD31 magnetic beads (Figures S5A and S5B). The ability of CD31⁺ BMECs to form vessel networks on Matrigel is shown in Figure S5C. We found that these Tie2⁺/CD31⁺ ECs turned into RFP⁺/GFP⁺ dual-positive cells and mineralized on culturing in StemPro osteogenic medium (Figure 3H).

RFP⁺ mouse lung endothelial cells can transition to GFP⁺ osteoblasts *in vitro*

To examine whether EC-to-OSB transition can occur in ECs from non-skeletal tissues, we digested lungs from DRM with collagenase II, plated the cells on gelatin-coated plates, and cultured the cells in EC growth medium to isolate mouse lung ECs (MLECs) (Figures 4A and 4B). When plated on Matrigel in EC growth medium, RFP⁺ MLECs exhibited EC properties, as they formed extensive vessel networks (Figure 4C, enlarged). They were subsequently treated with BMP4 in serum-free medium for 3 days, during which the RFP⁺ vessel networks disappeared and the cells around the vessel branching points aggregated into ball-like structures (Figure 4D, arrows). When these ball-like structures were incubated in osteogenic medium for 17 days, we observed the appearance of GFP positivity in the MLECs (Figure 4D). We also directly incubated MLECs isolated from lung tissue (from Figure 4B) in osteogenic medium for 21 days and found the appearance of GFP positivity in the RFP⁺ MLECs (Figure 4E). Although the osteogenic medium contains BMP2, treating with BMP4 further enhanced the transition to RFP⁺/GFP⁺ cells (Figure 4E). Alizarin Red staining showed the mineralization of the RFP⁺/GFP⁺ MLEC clusters (Figure 4E). Furthermore, CD31 magnetic bead-purified Tie2⁺/CD31⁺ ECs (Figures S5D and S5E) turned into RFP⁺/GFP⁺ dual-positive cells and

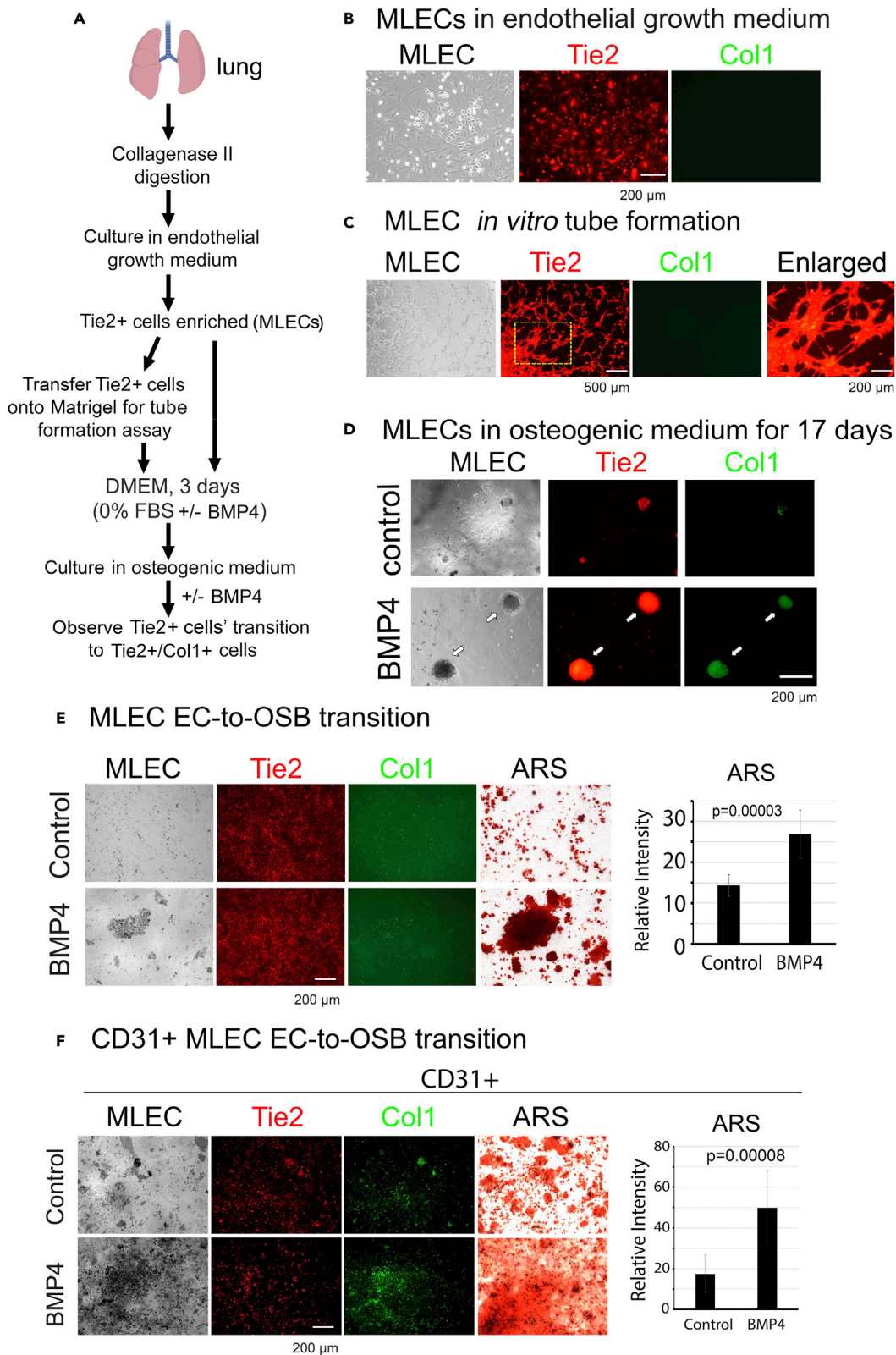


Figure 4. Transition of RFP⁺ lung endothelial cells to RFP⁺/GFP⁺ osteoblasts *in vitro*

(A) Procedure for isolating MLECs from DRM and inducing OSB transition.

(B) MLECs were RFP⁺ but GFP⁻.

(C) MLECs formed a tube structure in an endothelial tube formation assay. The boxed area in the RFP image is enlarged at right.

(D) MLECs in (C) were treated in serum-free DMEM for 3 days with or without BMP4 (100 ng/mL), during which the RFP⁺ vessel network disappeared and cells around the vessel branching points aggregated into ball-like structures; these were further incubated in osteogenic medium with or without BMP4 (100 ng/mL) for 17 days. Arrows, RFP⁺ ball-like structures became RFP⁺/GFP⁺.

(E and F) MLECs from (B) were cultured in osteogenic medium for 21 days with or without BMP4 (100 ng/mL). Media were refreshed twice weekly. Alizarin Red S (ARS) staining showed mineralized bone nodules in the RFP⁺/GFP⁺ MLEC clusters, and the staining was quantified using ImageJ software. Data are represented as mean ± SD (F) CD31⁺ MLECs were isolated from (B) using rat anti-mouse CD31 antibody-conjugated Dynabeads. Tie2⁺/CD31⁺ cells were subjected to *in vitro* osteogenic assays as described in (E). Data are represented as mean ± SD.

mineralized on culturing in StemPro osteogenic medium (Figure 4F). The ability of CD31⁺ MLECs to form vessel networks on Matrigel is shown in Figure S5F. These data demonstrate that RFP⁺ MLECs are capable of transitioning to RFP⁺/GFP⁺ OSBs when cultured in osteogenic medium, which suggests that EC-to-OSB transition also occurs in ECs from non-skeletal tissues *in vitro*.

RNA-sequencing analyses of RFP⁺ versus RFP⁺/GFP⁺ cells reveal transcriptomic changes during EC-to-OSB transition

We next compared the transcriptomes of RFP⁺ cells versus RFP⁺/GFP⁺ (EC-OSB) cells. Bone marrow cells were spun out of the femurs and tibias of two 3-month-old DRMs by centrifugation. The bone marrow cells were sorted by fluorescence-activated cell sorting (FACS) (Figure 5A). The distribution of RFP⁺, RFP⁺/GFP⁺ dual-positive, and GFP⁺ cells was found to be about 71.1%, 2.5%, and 0% of total pooled cells, respectively (Figure 5A). Thus, no GFP⁺ cells were collected from the bone marrow. The study was repeated with similar results.

RNAsequencing (RNAseq) analysis was performed on the sorted RFP⁺ and RFP⁺/GFP⁺ cells. Differential gene expression analysis was performed using DeSeq2 software, with a false discovery rate cutoff of 0.05 and a fold-change cutoff of 2, resulting in 644 upregulated genes and 525 downregulated genes (Table S1) (Gene Expression Omnibus accession number GSE207839). Gene set enrichment analysis (GSEA) using curated gene sets revealed upregulated matrisome, extracellular matrix, and collagen pathways in RFP⁺/GFP⁺ EC-OSB hybrid cells (Figure 5B). The top upregulated genes in RFP⁺/GFP⁺ cells relative to RFP⁺ cells included *Col1a1* and *2*, *Col11a1*, *Col5a2*, *Col14a1*, *Sparc*, *Dcn*, and *Lox* (Figure 5C), consistent with an increase in deposition of collagen and extracellular matrix during bone formation.^{22,23} Moreover, GSEA using hallmark gene sets identified epithelial-to-mesenchymal transition (EMT) among the top biological processes in RFP⁺/GFP⁺ EC-OSB hybrid cells (Figure 5D), consistent with similarities between EMT and endothelial-to-mesenchymal transition.²⁴ Of interest, GSEA using regulatory target gene sets identified multiple GATA gene signatures, including GATA_Q6, GATA_C, and GATA3_01, among the top 10 transcription factor gene signatures (Figure 5E).

The GATA family of transcription factors plays a role in multiple aspects of vertebrate development.^{25,26} GATA3 plays an important role in EC biology²⁷ and is an important regulator of development of T cells, including Th2^{28–30} and regulatory T cells.³¹ GATA4 was previously shown to be involved in OSB differentiation,³² neural crest and craniofacial skeleton development,³³ and tooth development.³⁴ GATA6 was shown to play a role in vertebrate chondrogenesis.³⁵ These studies suggest that distinct GATA family genes may be involved in EC-to-OSB transition. To examine which GATA family genes are involved, we examined the expression of six GATA family genes in MLECs and found that higher mRNA levels were detected for GATA3, 4, and 6 in MLECs (Figure 6A). However, only GATA3 and 4 expression were upregulated during BMP4-induced MLEC-to-OSB transition (Figure 6A). In 2H11, a lymphoid EC line³⁶ previously shown to undergo BMP4-induced EC-to-OSB transition,⁹ GATA3 expression was the most highly expressed GATA family gene. GATA3 expression was upregulated during BMP4-induced 2H11 EC-to-OSB transition (Figure 6B). These observations suggest that GATA3 may be involved in EC-to-OSB transition.

We next examined the role of GATA3 in EC-to-OSB transition using 2H11 ECs. We previously found that on BMP4 treatment, 2H11 ECs transition to OSBs by day 2–3 in serum-free medium and then undergo OSB differentiation and mineralization on days 3 through 20 in OSB differentiation medium.⁷ Notably, we found that GATA3 expression was highest during the early phase of EC-to-OSB transition (Figure 6C). Knockdown of GATA3 by shRNA, as shown by mRNA and protein levels (Figure 6D), significantly reduced BMP4-induced expression of *OSX* and osteocalcin (encoded by *Bglap*), which are reflective of EC-to-OSB transition (Figure 6E), and mineralization (Figure 6F). These results suggest that GATA3 plays a role in EC-to-OSB cell fate transition.

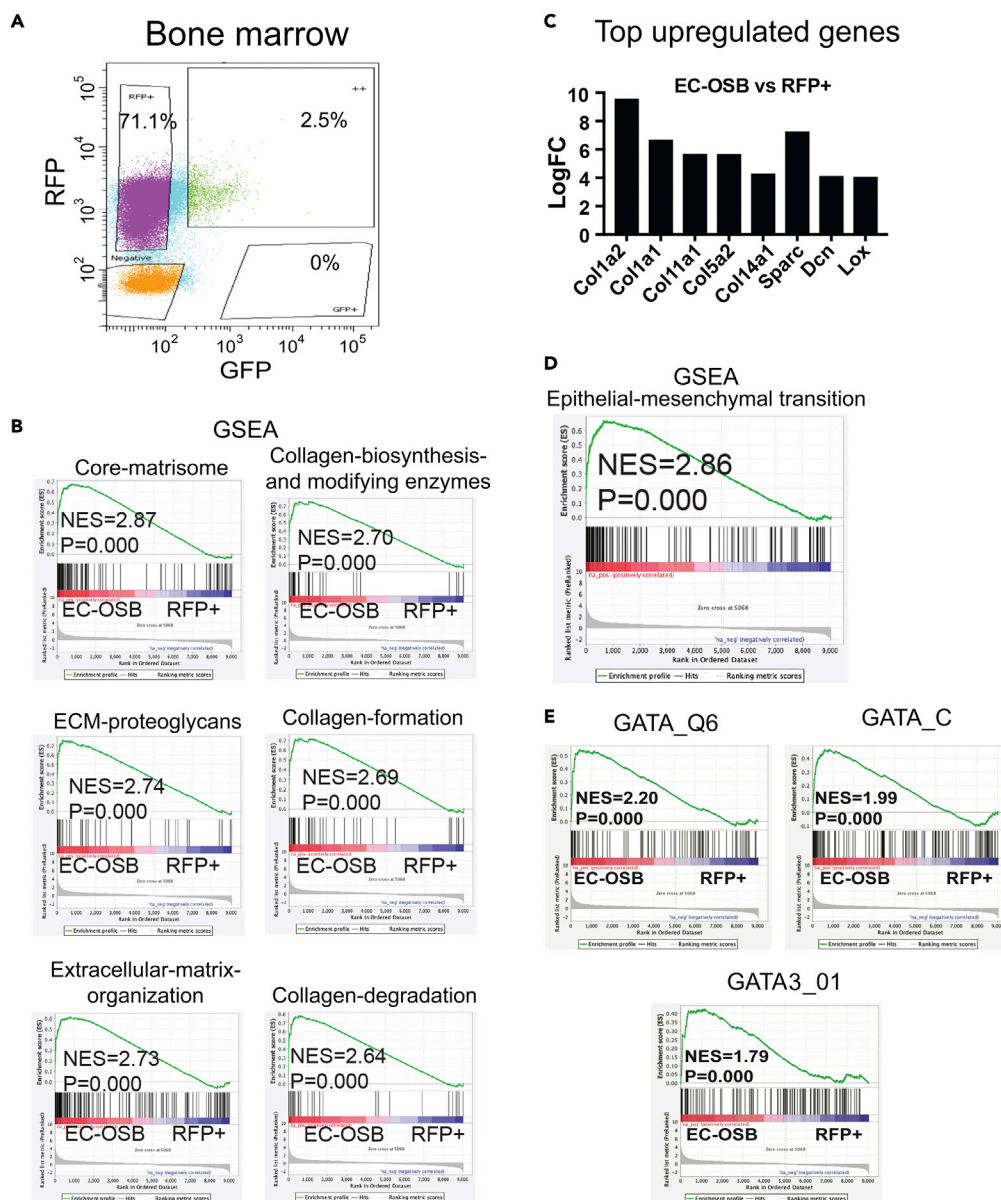


Figure 5. RNA-sequencing analysis of RFP⁺/GFP⁺ versus RFP⁺ cells

(A) Pooled bone marrow cells from DRM were sorted by FACS, and RFP⁺ and RFP⁺/GFP⁺ cells collected.

(B) GSEA of differentially expressed genes from RNAseq analyses of RFP⁺/GFP⁺ (EC-OSB) versus RFP⁺ cells. NES, normalized enrichment score.

(C) The top upregulated genes in RFP⁺/GFP⁺ (EC-OSB) cells relative to RFP⁺ cells.

(D) Hallmark gene set analysis identified EMT as among the top biological processes in RFP⁺/GFP⁺ cells.

(E) Regulatory target gene set analysis showed that GATA genes, including GATA_Q6, GATA_C, and GATA3_01, were among the top 10 transcription factor gene signatures.

DISCUSSION

Using lineage tracing, we showed that Tie2-RFP⁺ and Col1 α 1-GFP⁺ dual-positive cells are present in cells lining the bone. In addition, Tie2-RFP⁺ cells isolated from bone marrow or lungs were able to transition into Col1 α 1-GFP⁺ OSBs when cultured *in vitro*, as summarized in Figure 6G. Although several cell types, including bone marrow stromal cells³⁷ and adipocyte stem cells,³⁸ have been shown to be precursors of OSBs, our study provides evidence that ECs are also a cellular precursor of OSBs during normal bone formation. Our previous studies have shown that EC-to-OSB transition plays a role in PCa-induced bone

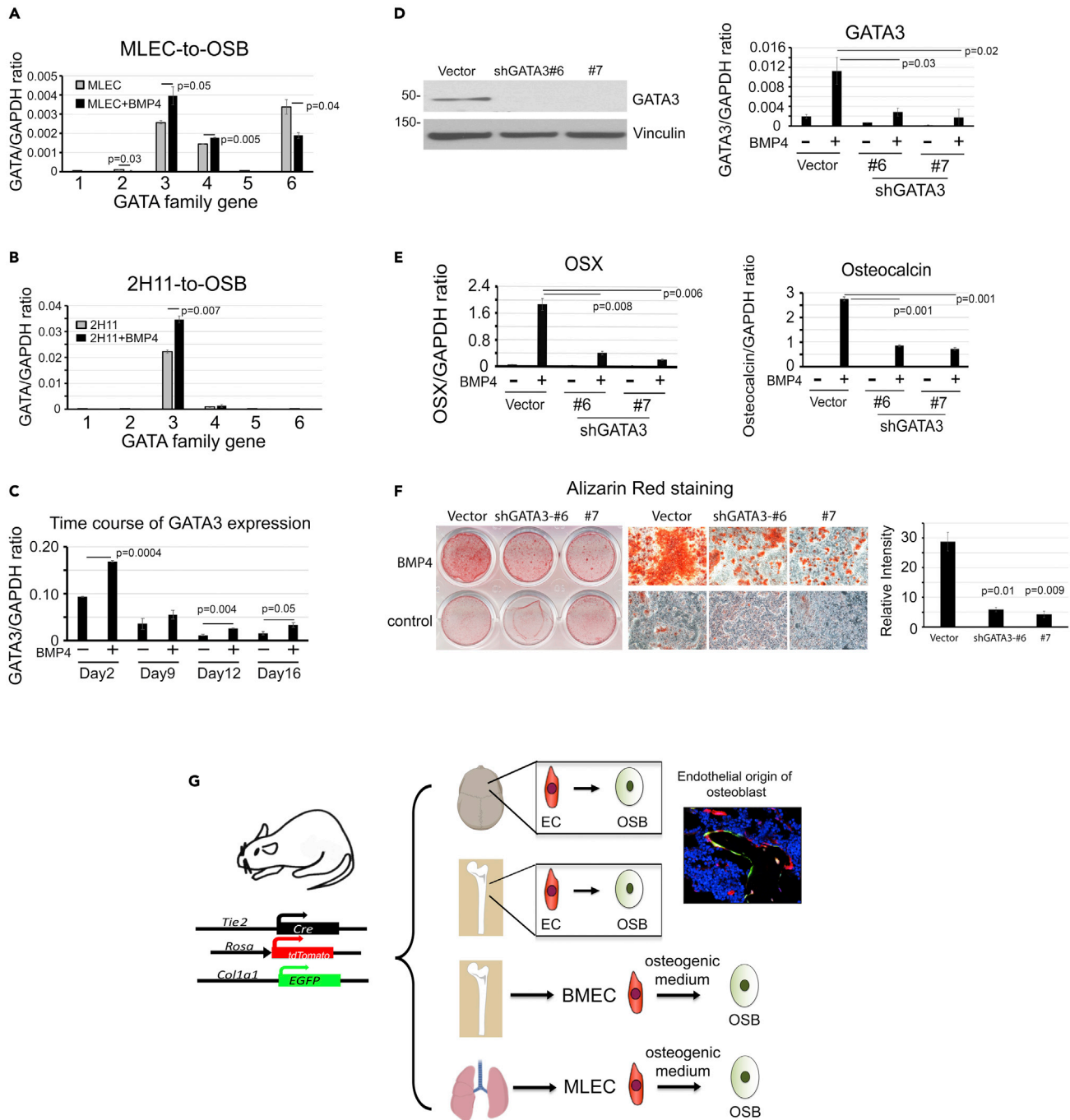


Figure 6. GATA3 transcription factor in endothelial-to-osteoblast transition

(A–C) qRT-PCR of MLEC mRNA for the expression of GATA family genes before and after BMP4 treatment for 14 days (B) GATA family gene expression in 2H11 ECs after BMP4 treatment for 2 days (C) Time course of GATA3 induction during BMP4-induced EC-to-OSB transition of 2H11 ECs. (D) Knockdown of GATA3 by shRNA in 2H11 ECs, as shown by mRNA and protein levels. (E) shRNA knockdown of GATA3 significantly reduced BMP4-induced OSX and osteocalcin (*Bglp*) expression in 2H11 cells. (F and G) Knockdown of GATA3 in 2H11 cells reduced BMP4-induced mineralization. Left panel, Alizarin Red S (ARS) staining. Right panel, enlarge image (X10) of left panel. The staining was quantified using ImageJ software. Data in A–E are represented as mean \pm SD (G) Graphical summary. Using lineage tracing, we showed that *Tie2*-RFP⁺ and *Col1 α 1*-GFP⁺ dual-positive cells are present in cells lining the calvaria bone, femur, and other bones. We also isolated ECs from bone marrow or lung of DRM and showed that they could become OSBs when cultured in osteogenic medium. These observations suggest that EC-to-OSB transition occurs during normal bone development.

formation in the metastatic progression of PCa in bone.³ Together, these results suggest that EC-to-OSB transition occurs in both normal bone development and pathological conditions. Our findings suggest a new paradigm that ECs participate in normal bone development, which has implications for both bone repair and bone metastasis treatments.

Although Tie2 is also expressed in other cell types, including hematopoietic cells^{39,40} and macrophages,⁴¹ we selected bone marrow or lung Tie2⁺ ECs by culturing cells in a gelatin-coated plate with EC growth medium. We also confirmed their endothelial properties by performing tube formation assays. In addition, we showed that Tie2⁺/CD31⁺ cells can become OSBs. Medici et al.⁴² also reported EC-to-OSB transition in human umbilical vein ECs and human cutaneous microvascular ECs *in vitro*. We previously showed that EC-to-OSB transition can occur in murine EC lines, including 2H11 and SVR.⁹ Together, these studies provide strong evidence that EC-to-OSB transition can occur *in vivo* as well as in primary ECs from various tissues and several EC lines.

In normal bone development, we found that only Tie2⁺ ECs located on the bone surface become OSBs, suggesting that the local environment plays a role in regulating cell-type transition. Because BMPs are enriched in bone tissue, it is possible that Tie2⁺ ECs located on the bone surface are stimulated by BMPs present in the bone microenvironment. Of interest, Gunne-Braden et al.⁴³ showed that GATA3 is an early commitment gene that mediates commitment to BMP4-driven differentiation of human embryonic stem cells. Our observation that GATA3 is among the top transcription factors upregulated in RFP⁺/GFP⁺ cells suggests that BMP4 likely plays a role in regulating EC-to-OSB transition *in vivo*. It is also possible that Tie2⁺ ECs that are localized on the bone surface have unique properties. For example, Sanchez-Duffhues et al.⁴⁴ reported that human and murine ECs lacking primary cilia are prone to undergo mineralization in response to BMP stimulation *in vitro*. These possibilities remain to be examined.

We observed different RFP/GFP ratios in EC-OSB hybrid cells both in isolated individual cells and in OSBs rimming the bone surfaces of calvariae or femurs. Although different RFP/GFP ratios may be because of differences in levels of expression from Tie2-Cre and Col1-GFP transgenes, we cannot exclude the possibility that different RFP/GFP ratios are attributable to different stages of EC-to-OSB transition. In E15.5 embryos, when blood vessels are entering the avascular cartilage and OSBs are starting to appear, the RFP⁺ cells may be undergoing different stages of EC-to-OSB transition, with a high RFP/GFP ratio in the early stage of EC-to-OSB transition and a low RFP/GFP ratio when the cells become more mature OSBs. A similar phenomenon was seen in femurs, in which OSBs on the bone surface exhibited different RFP/GFP ratios; these EC-OSB cells may be at different stages of EC-to-OSB transition. However, we also observed different RFP/GFP ratios in the circulating EC-OSB cells. Whether these circulating EC-OSB cells are released into circulation while they are undergoing different stages of EC-to-OSB transition is unknown.

Our studies demonstrate that Tie2⁺ ECs provide one source of OSBs. Other cell populations in the bone marrow, including NG2⁺ pericytes,⁴⁵ LepR⁺ cells,^{46,47} and Gli1⁺ cells,⁴⁸ have been reported to have osteogenic capacity. We also examined whether other RFP⁺ cells, e.g., CD31⁻ RFP⁺ cells, have capacity for OSB differentiation. We collected DRM bone marrow and lung RFP⁺ cells that did not bind to CD31-magnetic beads (CD31⁻ RFP⁺ cells) for an osteogenesis assay. We found that these CD31⁻ RFP⁺ cells were also able to form vessel structures in the tube formation assay. Upon culturing in OSB differentiation medium, these CD31⁻ RFP⁺ cells differentiated into OSBs and formed mineralized bone matrix (Figure S6). Bone marrow stromal cells (BMSCs or MSCs) have been shown to be a main source of OSBs.⁴⁹ To examine whether BMSCs have features similar to those of EC progenitors, we isolated BMSCs based on the procedure described by Soleimani and Nadri.²⁰ We found that BMSCs from DRM were RFP⁺ (Tie2⁺) (Figure S7). However, these RFP⁺ BMSCs did not form vessel networks in the tube formation assay (Figure S7). The RFP⁺ BMSCs were able to mineralize on culturing in osteogenic differentiation medium (Figure S7). These observations indicate that like ECs, BMSCs are Tie2⁺ and can form OSBs. However, BMSCs differed from ECs in that BMSCs did not exhibit the endothelial vessel-forming property. Thus, Tie2⁺ BMSCs, besides Tie2⁺ ECs, can be a source of OSBs.

Another interesting question is the relative contribution of BMSC-to-OSB differentiation and EC-to-OSB transition in the normal bone development process. Because OSBs could be generated from both Tie2⁺ ECs and Tie2⁺ BMSCs in our study model, the relative contribution of BMSC-to-OSB differentiation and EC-to-OSB transition in the normal bone development process cannot be determined. To determine the fraction of OSBs that are contributed from each source, strategies that distinguish OSBs from different progenitor sources will be needed.

Endothelial progenitor cells are capable of differentiating into multiple cell types through different signaling pathways.⁵⁰ Through endothelial-to-hematopoietic cell transition (EHT), endothelial cells transition to multi-lineage hematopoietic stem and progenitor cells. Endothelial cells can also acquire characteristics of fibroblasts, smooth muscle cells, osteocytes, adipocytes, and chondrocytes through endothelial-to-mesenchymal transition (EndMT).⁵⁰ It is of interest to know whether the signaling pathways leading to EC-to-OSB transition overlap with EHT or EndMT. During EHT, retinoic acid signaling, which leads upregulation of c-Kit and Notch,⁵⁰ is required for specification of hemogenic endothelial cells. In contrast, activation of the β -catenin, TGF β , and BMP pathways is implicated in EndMT. During EndMT, the ECs respond by partial downregulation of endothelial markers, followed by upregulation of mesenchymal markers, including matrix proteins, metalloproteases, or cytoskeletal proteins.⁵⁰ We have previously delineated the signaling pathways mediating EC-to-OSB transition in endothelial cell lines 2H11 and SVR.⁹ We found that for BMP4-induced EC-to-OSB transition to occur, inhibition of angiogenesis through the Smad1-Notch-Hey1 pathway plus activation of osteogenesis through the p38MAPK(p44/42ERK,AKT)-GSK3 β - β -catenin-Slug pathway are required. In addition, Smad1-regulated Dlx2 plays a role in converging the Smad1 and β -catenin pathways during EC-to-OSB transition.⁹ By comparing the signaling pathways of EC-to-OSB transition with those for EHT and EndMT, we found that EC-to-OSB transition shares similarity with those of EndMT, including the involvement of the β -catenin and BMP pathways and the secretion of matrix proteins, e.g., Tenascin C and fibronectin.⁷ Furthermore, we showed that retinoic acid signaling inhibits EC-to-OSB transition and may be used as a strategy to reduce the generation of aberrant bone formation from BMP4-stimulated EC-to-OSB transition.⁵¹ This is in contrast to the requirement of retinoic acid signaling for EHT.⁵⁰ Thus, the signaling pathways leading to EC-to-OSB transition overlap with EndMT.

Although we used GSEA to identify GATA transcription factors that were upregulated in EC-OSB hybrid cells compared to ECs, it would be interesting to know transcription factors that are downregulated in EC-to-OSB transition, which might be correlated with EC lineage specification and maintenance. To interrogate this, we used i-cisTarget software^{52,53} to analyze the potential transcription factors responsible for the downregulated genes from the RNAseq data. We identified IRF4, MEF2A, TCF12, MyoD, ETS1, EP300, TCF3, and CHD1 as candidates. Some of these genes have been implicated in lineage differentiation. For example, Irf4 was shown to regulate T cell differentiation by preventing T lymphoid-primed progenitors from adopting the myeloid fate.⁵⁴ MEF2A plays an important role in neural stem cell differentiation.⁵⁵ TCF12 downregulation plays an essential role in the osteogenic differentiation of bone marrow mesenchymal stem cells.⁵⁶ MyoD is required for myogenic determination during early embryogenesis.⁵⁷ ETS1 plays a role in the differentiation of human hematopoietic progenitor cells into megakaryocytic differentiation by suppressing erythroid differentiation.⁵⁸ ETS1 is also involved in the lineage differentiation of CD8 T cells.⁵⁹ The roles of these transcription factors in EC-to-OSB transition will be examined in our future studies.

A role of ECs in supporting osteogenesis has been reported by Kusumbe et al.,⁶⁰ who showed that a specialized capillary EC subtype, termed type H, coupled angiogenesis and osteogenesis in adolescent, adult, and aging mice.⁶⁰ In contrast, embryonic and early postnatal long bone contains a specialized EC subtype, termed type E, that supports OSB lineage cells.⁶¹ These studies suggest that ECs play a role in supporting osteogenesis; however, whether some of these ECs can become OSBs was not addressed. Our studies showed that a fraction of Tie2⁺ ECs can become OSBs that can mineralize to form bone. It is not clear how the Tie2⁺ ECs in our study compare to the specialized EC subtypes.^{60,61} Nevertheless, these studies suggest that ECs play a critical role in OSB formation, directly or indirectly.

In conclusion, we have demonstrated that ECs are a source for OSBs in normal bone development. This new understanding of bone formation may contribute to the development of strategies for treating various bone diseases.

Limitations of the study

Although Tie2 is expressed in ECs, Tie2 is an early promoter and also expressed in hematopoietic cells and many other cell types.⁴⁰ A more endothelial-specific marker, e.g., vascular endothelial (VE)-cadherin,⁶² may be considered. Similarly, the 2.3-kb Col1 α 1 promoter is an early promoter and collagens are expressed in pre-OSB and OSB stages.¹² However, a late promoter may not capture the transition that occurs during the early lineage commitment. Further study will be required to address these issues.

STAR★METHODS

Detailed methods are provided in the online version of this paper and include the following:

- **KEY RESOURCES TABLE**
- **RESOURCE AVAILABILITY**
 - Lead contact
 - Materials availability
 - Data and code availability
- **EXPERIMENTAL MODEL AND SUBJECT DETAILS**
- **METHOD DETAILS**
 - Generation of dual-reporter mice
 - Embryo collection and histology
 - Postnatal skeletal tissue collection and histology
 - Isolation of EC-OSB hybrid cells from calvariae
 - Isolation of bone marrow endothelial cells
 - Isolation of mouse lung endothelial cells
 - *In vitro* tube formation of BMECs and MLECs
 - *In vitro* osteogenic differentiation assays for BMECs and MLECs
 - Isolation of CD31⁺ cells from MLECs and BMECs
 - FACS and RNAseq analysis
 - GATA gene family analysis
- **QUANTIFICATION AND STATISTICAL ANALYSIS**

SUPPLEMENTAL INFORMATION

Supplemental information can be found online at <https://doi.org/10.1016/j.isci.2023.105994>.

ACKNOWLEDGMENTS

The authors would like to acknowledge Sunita Patterson in MD Anderson's Research Medical Library for editing the manuscript. This work was supported by grants from the NIH R01CA174798 (S.-H. Lin, L.-Y. Yu-Lee), NIH 5P50CA140388 (C. Logothetis, S.-H. Lin), and NIH P30CA16672 Core grant to MD Anderson Cancer Center; DoD [DOD-PCRP-Idea W81XWH-21-1-0522(GW)]; and Cancer Prevention Research Institute of Texas RP150179 and RP190252 (S.-H. Lin and L.-Y. Yu-Lee). This study was also supported by philanthropic contributions to The University of Texas MD Anderson Cancer Center Prostate cancer Moon Shot Program.

AUTHOR CONTRIBUTIONS

Conceptualization: S.-H.L.; Methodology; S.-C.L.; Investigation: S.-C.L., Y.-C.L., G.Y., and J.H.S.; Data analysis and interpretation: X.S., J.Z., T.P., G.W., Y.K., and S.-H.L.; Writing – Original Draft: G.W. and S.-H.L.; Writing – Review and Editing: S.-H.L., S.-C.L., L.-Y.Y.-L., and Y.K.; Funding Acquisition: C.J.L., S.-H.L., G.W., L.-Y.Y.-L.; Supervision: G.W., S.-H.L. All coauthors critically reviewed the present manuscript before submission.

DECLARATION OF INTERESTS

The authors declare no competing interests.

Received: August 9, 2022

Revised: December 23, 2022

Accepted: January 12, 2023

Published: February 17, 2023

REFERENCES

1. Logothetis, C.J., and Lin, S.-H. (2005). Osteoblasts in prostate cancer metastasis to bone. *Nat. Rev. Cancer* 5, 21–28.
2. Lee, Y.C., Cheng, C.J., Bilen, M.A., Lu, J.F., Satcher, R.L., Yu-Lee, L.Y., Gallick, G.E., Maity, S.N., and Lin, S.H. (2011). BMP4 promotes prostate tumor growth in bone through osteogenesis. *Cancer Res.* 71, 5194–5203. <https://doi.org/10.1158/0008-5472.CAN-10-4374>.
3. Lin, S.C., Lee, Y.C., Yu, G., Cheng, C.J., Zhou, X., Chu, K., Murshed, M., Le, N.T., Baseler, L., Abe, J.I., et al. (2017). Endothelial-to-Osteoblast conversion generates osteoblastic metastasis of prostate cancer. *Dev. Cell* 41, 467–480.e3. <https://doi.org/10.1016/j.devcel.2017.05.005>.
4. Nordstrand, A., Bovinder Ylitalo, E., Thysell, E., Jernberg, E., Crnalic, S., Widmark, A., Bergh, A., Lerner, U.H., and Wikström, P. (2018). Bone cell activity in clinical prostate

- cancer bone metastasis and its inverse relation to tumor cell androgen receptor activity. *Int. J. Mol. Sci.* **19**, 1223. <https://doi.org/10.3390/ijms19041223>.
5. Dai, J., Keller, J., Zhang, J., Lu, Y., Yao, Z., and Keller, E.T. (2005). Bone morphogenetic protein-6 promotes osteoblastic prostate cancer bone metastases through a dual mechanism. *Cancer Res.* **65**, 8274–8285.
 6. Lee, Y.C., Lin, S.C., Yu, G., Cheng, C.J., Liu, B., Liu, H.C., Hawke, D.H., Parikh, N.U., Varkaris, A., Corn, P., et al. (2015). Identification of bone-derived factors conferring de novo therapeutic resistance in metastatic prostate cancer. *Cancer Res.* **75**, 4949–4959. <https://doi.org/10.1158/0008-5472.CAN-15-1215>.
 7. Lee, Y.C., Lin, S.C., Yu, G., Zhu, M., Song, J.H., Rivera, K., Pappin, D.J., Logothetis, C.J., Panaretakis, T., Wang, G., et al. (2022). Prostate tumor-induced stromal reprogramming generates Tenascin C that promotes prostate cancer metastasis through YAP/TAZ inhibition. *Oncogene* **41**, 757–769. <https://doi.org/10.1038/s41388-021-02131-7>.
 8. Roudier, M.P., Morrissey, C., True, L.D., Higano, C.S., Vessella, R.L., and Ott, S.M. (2008). Histopathological assessment of prostate cancer bone osteoblastic metastases. *J. Urol.* **180**, 1154–1160.
 9. Yu, G., Shen, P., Lee, Y.C., Pan, J., Song, J.H., Pan, T., Lin, S.C., Liang, X., Wang, G., Panaretakis, T., et al. (2021). Multiple pathways coordinating reprogramming of endothelial cells into osteoblasts by BMP4. *iScience* **24**, 102388. <https://doi.org/10.1016/j.isci.2021.102388>.
 10. Kisanuki, Y.Y., Hammer, R.E., Miyazaki, J., Williams, S.C., Richardson, J.A., and Yanagisawa, M. (2001). Tie2-Cre transgenic mice: a new model for endothelial cell-lineage analysis in vivo. *Dev. Biol.* **230**, 230–242. <https://doi.org/10.1006/dbio.2000.0106>.
 11. Schnürch, H., and Risau, W. (1993). Expression of tie-2, a member of a novel family of receptor tyrosine kinases, in the endothelial cell lineage. *Development* **119**, 957–968. <https://doi.org/10.1242/dev.119.3.957>.
 12. Aubin, J.E. (1998). Advances in the osteoblast lineage. *Biochem. Cell. Biol.* **76**, 899–910.
 13. Dumont, D.J., Fong, G.H., Puri, M.C., Gradwohl, G., Alitalo, K., and Breitman, M.L. (1995). Vascularization of the mouse embryo: a study of flk-1, tek, tie, and vascular endothelial growth factor expression during development. *Dev. Dyn.* **203**, 80–92. <https://doi.org/10.1002/aja.1002030109>.
 14. Rossert, J., Eberspaecher, H., and de Crombrughe, B. (1995). Separate cis-acting DNA elements of the mouse pro- α 1(I) collagen promoter direct expression of reporter genes to different type I collagen-producing cells in transgenic mice. *J. Cell Biol.* **129**, 1421–1432.
 15. Drake, C.J., and Fleming, P.A. (2000). Vasculogenesis in the day 6.5 to 9.5 mouse embryo. *Blood* **95**, 1671–1679.
 16. Walls, J.R., Coultas, L., Rossant, J., and Henkelman, R.M. (2008). Three-dimensional analysis of vascular development in the mouse embryo. *PLoS One* **3**, e2853. <https://doi.org/10.1371/journal.pone.0002853>.
 17. Kozhemyakina, E., Lassar, A.B., and Zelzer, E. (2015). A pathway to bone: signaling molecules and transcription factors involved in chondrocyte development and maturation. *Development* **142**, 817–831. <https://doi.org/10.1242/dev.105536>.
 18. Eghbali-Fatourehchi, G.Z., Lamsam, J., Fraser, D., Nagel, D., Riggs, B.L., and Khosla, S. (2005). Circulating osteoblast-lineage cells in humans. *N. Engl. J. Med.* **352**, 1959–1966.
 19. Suriyachand, K., Eamwijit, T., Paisooksantivatana, K., Hongeng, S., and Bunyaratavej, N. (2011). A study of correlation of osteoblasts from peripheral blood with related bone turnover markers. *J. Med. Assoc. Thai.* **94**, S71–S75.
 20. Soleimani, M., and Nadri, S. (2009). A protocol for isolation and culture of mesenchymal stem cells from mouse bone marrow. *Nat. Protoc.* **4**, 102–106. <https://doi.org/10.1038/nprot.2008.221>.
 21. Almeida-Porada, G., and Ascensão, J.L. (1996). Isolation, characterization, and biologic features of bone marrow endothelial cells. *J. Lab. Clin. Med.* **128**, 399–407.
 22. Rosset, E.M., and Bradshaw, A.D. (2016). SPARC/osteonection in mineralized tissue. *Matrix Biol.* **52–54**, 78–87. <https://doi.org/10.1016/j.matbio.2016.02.001>.
 23. Rutkovskiy, A., Stensløkken, K.O., and Vaage, I.J. (2016). Osteoblast differentiation at a glance. *Med. Sci. Monit. Basic Res.* **22**, 95–106. <https://doi.org/10.12659/msmbr.901142>.
 24. Saito, A. (2013). EMT and EndMT: regulated in similar ways? *J. Biochem.* **153**, 493–495. <https://doi.org/10.1093/jb/mvt032>.
 25. Bresnick, E.H., Martowicz, M.L., Pal, S., and Johnson, K.D. (2005). Developmental control via GATA factor interplay at chromatin domains. *J. Cell. Physiol.* **205**, 1–9. <https://doi.org/10.1002/jcp.20393>.
 26. Peterkin, T., Gibson, A., Loose, M., and Patient, R. (2005). The roles of GATA-4, -5 and -6 in vertebrate heart development. *Semin. Cell Dev. Biol.* **16**, 83–94. <https://doi.org/10.1016/j.semcdb.2004.10.003>.
 27. Song, H., Suehiro, J.i., Kanki, Y., Kawai, Y., Inoue, K., Daida, H., Yano, K., Ohhashi, T., Oettgen, P., Aird, W.C., et al. (2009). Critical role for GATA3 in mediating Tie2 expression and function in large vessel endothelial cells. *J. Biol. Chem.* **284**, 29109–29124. <https://doi.org/10.1074/jbc.M109.041145>.
 28. George, K.M., Leonard, M.W., Roth, M.E., Lieu, K.H., Kiousis, D., Grosveld, F., and Engel, J.D. (1994). Embryonic expression and cloning of the murine GATA-3 gene. *Development* **120**, 2673–2686. <https://doi.org/10.1242/dev.120.9.2673>.
 29. Ho, I.C., Vorhees, P., Marin, N., Oakley, B.K., Tsai, S.F., Orkin, S.H., and Leiden, J.M. (1991). Human GATA-3: a lineage-restricted transcription factor that regulates the expression of the T cell receptor alpha gene. *EMBO J.* **10**, 1187–1192.
 30. Zheng, W., and Flavell, R.A. (1997). The transcription factor GATA-3 is necessary and sufficient for Th2 cytokine gene expression in CD4 T cells. *Cell* **89**, 587–596. [https://doi.org/10.1016/s0092-8674\(00\)80240-8](https://doi.org/10.1016/s0092-8674(00)80240-8).
 31. Wang, Y., Su, M.A., and Wan, Y.Y. (2011). An essential role of the transcription factor GATA-3 for the function of regulatory T cells. *Immunity* **35**, 337–348. <https://doi.org/10.1016/j.immuni.2011.08.012>.
 32. Zhou, T., Guo, S., Zhang, Y., Weng, Y., Wang, L., and Ma, J. (2017). GATA4 regulates osteoblastic differentiation and bone remodeling via p38-mediated signaling. *J. Mol. Histol.* **48**, 187–197. <https://doi.org/10.1007/s10735-017-9719-2>.
 33. Guo, S., Zhang, Y., Zhou, T., Wang, D., Weng, Y., Chen, Q., Ma, J., Li, Y.P., and Wang, L. (2018). GATA4 as a novel regulator involved in the development of the neural crest and craniofacial skeleton via Barx1. *Cell Death Differ.* **25**, 1996–2009. <https://doi.org/10.1038/s41418-018-0083-x>.
 34. Guo, S., Zhang, Y., Zhou, T., Wang, D., Weng, Y., Wang, L., and Ma, J. (2017). Role of GATA binding protein 4 (GATA4) in the regulation of tooth development via GNAI3. *Sci. Rep.* **7**, 1534. <https://doi.org/10.1038/s41598-017-01689-1>.
 35. Alexandrovich, A., Qureishi, A., Coudert, A.E., Zhang, L., Grigoriadis, A.E., Shah, A.M., Brewer, A.C., and Pizzey, J.A. (2008). A role for GATA-6 in vertebrate chondrogenesis. *Dev. Biol.* **314**, 457–470. <https://doi.org/10.1016/j.ydbio.2007.12.001>.
 36. Walter-Yohrling, J., Morgenbesser, S., Rouleau, C., Bagley, R., Callahan, M., Weber, W., and Teicher, B.A. (2004). Murine endothelial cell lines as models of tumor endothelial cells. *Clin. Cancer Res.* **10**, 2179–2189.
 37. Caplan, A.I. (1991). Mesenchymal stem cells. *J. Orthop. Res.* **9**, 641–650. <https://doi.org/10.1002/jor.1100090504>.
 38. Tabatabai, T.S., Haji-Ghasem-Kashani, M., and Nasiri, M. (2021). In vitro osteogenic induction of human adipose stem cells co-treated with betaine/osteogenesis differentiation medium. *Mol. Biol. Res. Commun.* **10**, 93–103. <https://doi.org/10.22099/mbr.2021.39354.1578>.
 39. Arai, F., Hirao, A., Ohmura, M., Sato, H., Matsuoka, S., Takubo, K., Ito, K., Koh, G.Y., and Suda, T. (2004). Tie2/angiopoietin-1 signaling regulates hematopoietic stem cell quiescence in the bone marrow niche. *Cell* **118**, 149–161. <https://doi.org/10.1016/j.cell.2004.07.004>.
 40. Tang, Y., Harrington, A., Yang, X., Friesel, R.E., and Liaw, L. (2010). The contribution of the Tie2+ lineage to primitive and definitive

- hematopoietic cells. *Genesis* 48, 563–567. <https://doi.org/10.1002/dvg.20654>.
41. Chen, L., Li, J., Wang, F., Dai, C., Wu, F., Liu, X., Li, T., Glauben, R., Zhang, Y., Nie, G., et al. (2016). Tie2 expression on macrophages is required for blood vessel reconstruction and tumor relapse after chemotherapy. *Cancer Res.* 76, 6828–6838. <https://doi.org/10.1158/0008-5472.CAN-16-1114>.
 42. Medici, D., Shore, E.M., Lounev, V.Y., Kaplan, F.S., Kalluri, R., and Olsen, B.R. (2010). Conversion of vascular endothelial cells into multipotent stem-like cells. *Nat. Med.* 16, 1400–1406. <https://doi.org/10.1038/nm.2252>.
 43. Gunne-Braden, A., Sullivan, A., Gharibi, B., Sheriff, R.S.M., Maity, A., Wang, Y.F., Edwards, A., Jiang, M., Howell, M., Goldstone, R., et al. (2020). GATA3 mediates a fast, irreversible commitment to BMP4-driven differentiation in human embryonic stem cells. *Cell Stem Cell* 26, 693–706.e9. <https://doi.org/10.1016/j.stem.2020.03.005>.
 44. Sánchez-Duffhues, G., de Vinuesa, A.G., Lindeman, J.H., Mulder-Stapel, A., DeRuiter, M.C., Van Munsteren, C., Goumans, M.J., Hierck, B.P., and Ten Dijke, P. (2015). SLUG is expressed in endothelial cells lacking primary cilia to promote cellular calcification. *Arterioscler.Thromb.Vasc. Biol.* 35, 616–627. <https://doi.org/10.1161/ATVBAHA.115.305268>.
 45. Supakul, S., Yao, K., Ochi, H., Shimada, T., Hashimoto, K., Sunamura, S., Mabuchi, Y., Tanaka, M., Akazawa, C., Nakamura, T., et al. (2019). Pericytes as a source of osteogenic cells in bone fracture healing. *Int. J. Mol. Sci.* 20, 1079. <https://doi.org/10.3390/ijms20051079>.
 46. Yen, Y.T., Chien, M., Wu, P.Y., and Hung, S.C. (2021). PP2A in LepR+ mesenchymal stem cells contributes to embryonic and postnatal endochondral ossification through Runx2 dephosphorylation. *Commun.Biol.* 4, 658. <https://doi.org/10.1038/s42003-021-02175-1>.
 47. Zhou, B.O., Yue, R., Murphy, M.M., Peyser, J.G., and Morrison, S.J. (2014). Leptin-receptor-expressing mesenchymal stromal cells represent the main source of bone formed by adult bone marrow. *Cell Stem Cell* 15, 154–168. <https://doi.org/10.1016/j.stem.2014.06.008>.
 48. Shi, Y., He, G., Lee, W.C., McKenzie, J.A., Silva, M.J., and Long, F. (2017). Gli1 identifies osteogenic progenitors for bone formation and fracture repair. *Nat. Commun.* 8, 2043. <https://doi.org/10.1038/s41467-017-02171-2>.
 49. Chan, C.K.F., Seo, E.Y., Chen, J.Y., Lo, D., McArdle, A., Sinha, R., Tevlin, R., Seita, J., Vincent-Tompkins, J., Wearada, T., et al. (2015). Identification and specification of the mouse skeletal stem cell. *Cell* 160, 285–298. <https://doi.org/10.1016/j.cell.2014.12.002>.
 50. Dejana, E., Hirschi, K.K., and Simons, M. (2017). The molecular basis of endothelial cell plasticity. *Nat. Commun.* 8, 14361. <https://doi.org/10.1038/ncomms14361>.
 51. Yu, G., Corn, P.G., Shen, P., Song, J.H., Lee, Y.C., Lin, S.C., Pan, J., Agarwal, S.K., Panaretakis, T., Pacifici, M., et al. (2022). Retinoic acid receptor activation reduces metastatic prostate cancer bone lesions by blocking the endothelial-to-osteoblast transition. *Cancer Res.* 82, 3158–3171. <https://doi.org/10.1158/0008-5472.CAN-22-0170>.
 52. Herrmann, C., Van de Sande, B., Potier, D., and Aerts, S. (2012). i-cisTarget: an integrative genomics method for the prediction of regulatory features and cis-regulatory modules. *Nucleic Acids Res.* 40, e114. <https://doi.org/10.1093/nar/gks543>.
 53. Imrichová, H., Hulselms, G., Atak, Z.K., Potier, D., and Aerts, S. (2015). i-cisTarget 2015 update: generalized cis-regulatory enrichment analysis in human, mouse and fly. *Nucleic Acids Res.* 43, W57–W64. <https://doi.org/10.1093/nar/gkv395>.
 54. Wang, S., He, Q., Ma, D., Xue, Y., and Liu, F. (2015). Irf4 regulates the choice between T lymphoid-primed progenitor and myeloid lineage fates during embryogenesis. *Dev. Cell* 34, 621–631. <https://doi.org/10.1016/j.devcel.2015.07.011>.
 55. Zhu, B., Carmichael, R.E., Solabre Valois, L., Wilkinson, K.A., and Henley, J.M. (2018). The transcription factor MEF2A plays a key role in the differentiation/maturation of rat neural stem cells into neurons. *Biochem.Biophys. Res. Commun.* 500, 645–649. <https://doi.org/10.1016/j.bbrc.2018.04.125>.
 56. Yi, S., Yu, M., Yang, S., Miron, R.J., and Zhang, Y. (2017). Tcf12, A member of basic helix-loop-helix transcription factors, mediates bone marrow mesenchymal stem cell osteogenic differentiation in vitro and in vivo. *Stem Cells* 35, 386–397. <https://doi.org/10.1002/stem.2491>.
 57. Berkes, C.A., and Tapscott, S.J. (2005). MyoD and the transcriptional control of myogenesis. *Semin. Cell Dev. Biol.* 16, 585–595. <https://doi.org/10.1016/j.semdb.2005.07.006>.
 58. Lulli, V., Romania, P., Morsilli, O., Gabbianelli, M., Pagliuca, A., Mazzeo, S., Testa, U., Peschle, C., and Marziani, G. (2006). Overexpression of Ets-1 in human hematopoietic progenitor cells blocks erythroid and promotes megakaryocytic differentiation. *Cell Death Differ.* 13, 1064–1074. <https://doi.org/10.1038/sj.cdd.4401811>.
 59. Zamisch, M., Tian, L., Grenningloh, R., Xiong, Y., Wildt, K.F., Ehlers, M., Ho, I.C., and Bosselut, R. (2009). The transcription factor Ets1 is important for CD4 repression and Runx3 up-regulation during CD8 T cell differentiation in the thymus. *J. Exp. Med.* 206, 2685–2699. <https://doi.org/10.1084/jem.20092024>.
 60. Kusumbe, A.P., Ramasamy, S.K., and Adams, R.H. (2014). Coupling of angiogenesis and osteogenesis by a specific vessel subtype in bone. *Nature* 507, 323–328. <https://doi.org/10.1038/nature13145>.
 61. Langen, U.H., Pitulescu, M.E., Kim, J.M., Enriquez-Gasca, R., Sivaraj, K.K., Kusumbe, A.P., Singh, A., Di Russo, J., Bixel, M.G., Zhou, B., et al. (2017). Cell-matrix signals specify bone endothelial cells during developmental osteogenesis. *Nat. Cell Biol.* 19, 189–201. <https://doi.org/10.1038/ncb3476>.
 62. Vestweber, D. (2008). VE-cadherin: the major endothelial adhesion molecule controlling cellular junctions and blood vessel formation. *Arterioscler.Thromb.Vasc. Biol.* 28, 223–232. <https://doi.org/10.1161/ATVBAHA.107.158014>.
 63. Dobin, A., Davis, C.A., Schlesinger, F., Drenkow, J., Zaleski, C., Jha, S., Batut, P., Chaisson, M., and Gingeras, T.R. (2013). STAR: ultrafast universal RNA-seq aligner. *Bioinformatics* 29, 15–21. <https://doi.org/10.1093/bioinformatics/bts635>.
 64. Anders, S., Pyl, P.T., and Huber, W. (2015). HTSeq—a Python framework to work with high-throughput sequencing data. *Bioinformatics* 31, 166–169. <https://doi.org/10.1093/bioinformatics/btu638>.
 65. Love, M.I., Huber, W., and Anders, S. (2014). Moderated estimation of fold change and dispersion for RNA-seq data with DESeq2. *Genome Biol.* 15, 550. <https://doi.org/10.1186/s13059-014-0550-8>.
 66. Subramanian, A., Tamayo, P., Mootha, V.K., Mukherjee, S., Ebert, B.L., Gillette, M.A., Paulovich, A., Pomeroy, S.L., Golub, T.R., Lander, E.S., and Mesirov, J.P. (2005). Gene set enrichment analysis: a knowledge-based approach for interpreting genome-wide expression profiles. *Proc. Natl. Acad. Sci. USA* 102, 15545–15550. <https://doi.org/10.1073/pnas.0506580102>.
 67. Mootha, V.K., Lindgren, C.M., Eriksson, K.F., Subramanian, A., Sihag, S., Lehar, J., Puigserver, P., Carlsson, E., Ridderstråle, M., Laurila, E., et al. (2003). PGC-1alpha-responsive genes involved in oxidative phosphorylation are coordinately downregulated in human diabetes. *Nat. Genet.* 34, 267–273. <https://doi.org/10.1038/ng1180>.

STAR★METHODS

KEY RESOURCES TABLE

REAGENT or RESOURCE	SOURCE	IDENTIFIER
Antibodies		
GATA3	R&D Systems	MAB6330-S, RRID: AB_10640
GAPDH(D16H11)	Cell Signaling Technologies	#5174, RRID:AB_10622025
Rat anti-mCD31 (MEC 13.3)	BD Pharmingen	#553370
Chemicals, peptides, and recombinant proteins		
BD Matrigel growth factor reduced	BD Biosciences	#354230
Dynabead-sheep anti-rat IgG	Life Technologies	#11035
Recombinant human BMP4	R&D Systems	314-BP
Critical commercial assays		
StemPro osteogenesis differentiation kit	Life Technologies	A10072-01
Endothelial cell growth supplement (ECGS)	Sigma	#02-101
Deposited data		
Raw and analyzed data		GEO: GSE207839
Experimental models: Cell lines		
2H11 mouse lymphoid endothelial cells	ATCC	#CRL-2163, RRID: CVCL_6762
Col1 α 1-GFP transgenic mice, B6.Cg-Tg(Col1a1*2.3-GFP)1Rowe/J	Jackson Laboratory	#013134, RRID:IMSR_JAX:013134
Tie2-Cre transgenic mice, B6.Cg-Tg(Tek-cre)12Flv/J,	Jackson Laboratory	#004128, RRID:IMSR_JAX:004128
Rosa-tdTomato (RFP) mice, B6.Cg-Gt(ROSA)26Sor ^{tm14(CAG-tdTomato)Hze/J}	Jackson Laboratory	#007914, RRID:IMSR_JAX:007914

RESOURCE AVAILABILITY

Lead contact

Further information and requests for resources and reagents should be directed to and will be fulfilled by the lead contact, Sue-Hwa Lin (slin@mdanderson.org).

Materials availability

This study did not generate new unique reagents.

Data and code availability

- All data reported in this paper will be shared by the [lead contact](#) upon request.
- This paper does not report original code.
- Any additional information required to reanalyze the data reported in this paper is available from the [lead contact](#) upon request.

EXPERIMENTAL MODEL AND SUBJECT DETAILS

Animals All animal procedures were conducted in accordance with the National Institutes of Health Guide for the Care and Use of Laboratory Animals and approved by Institutional Animal Care and Use Committee (approval No. 00000926-RN03). All efforts were made to minimize animal suffering and discomfort and to reduce the number of animals used. Experiments were performed using E15.5 and 1–6-month-old male and female mice.

METHOD DETAILS

Generation of dual-reporter mice

The Col1 α 1-GFP/Tie2-Cre/Rosa-tdTomato DRM were generated by crossing Col1 α 1-GFP transgenic mice (Jackson Laboratory #013134), Tie2-Cre transgenic mice (Jackson Lab #004128), and Rosa-tdTomato (RFP) mice (Jackson Laboratory #007914). Mice were the C57BL/6 strain. The Rosa-tdTomato mice were first bred with female Tie2-Cre mice to generate Tie2-Cre/Rosa-tdTomato (RFP reporter) mice. Female RFP reporter mice were mated with Col1 α 1-GFP mice to generate DRM mice. All the mouse strains and other key reagents used in this study are listed in [key resources table](#). Primer sequences used are listed in [Table S2](#).

Mouse manipulations were approved by the MD Anderson Cancer Center Institutional Animal Care and Use Committee.

Embryo collection and histology

Based on the timed pregnancy, embryos at various stages were collected from the breeding of DRM, and the plug date was counted as embryonic day 0.5 post coitum (E0.5). We obtained two DRM embryos at E15.5. These embryos were dissected, and skeletal tissues, including the head, frontal and parietal calvariae, and hind limbs, were collected. Embryonic tissues were fixed in 4% paraformaldehyde (PFA) at 4°C, equilibrated in sucrose gradients, and embedded in OCT for frozen blocks. The blocks were cut into 5- μ m sections, processed, and counterstained with DAPI for histological analysis. Images were taken using either an Olympus IX71, Leica DMI8 (with z-step focus), or Leica SP8 confocal fluorescence microscope.

Postnatal skeletal tissue collection and histology

Three 1-month-old and two 6-month-old DRM were dissected, and the calvariae, femurs, and tibias were collected. Bones were fixed in 4% PFA and decalcified in 0.25M EDTA at 4°C. Skeletal tissues were prepared and processed for histological analysis, and images were taken as described above.

Isolation of EC-OSB hybrid cells from calvariae

Calvariae of two 3-month-old DRM were dissected, attached soft membrane removed, and calvariae digested with trypsin/EDTA for 10 min. Cells released into the supernatant were discarded. Subsequently, bones were subjected to two consecutive rounds of digestion in 0.2% collagenase II solution at 37°C for 1 h each. The two supernatants were pooled and filtered through a 70- μ m mesh, and cells were collected. Blood was drawn from DRM, and red blood cells were lysed in NH₄Cl lysis buffer. Isolated cells were stained with DAPI and spotted on microscope slides for fluorescent imaging.

Isolation of bone marrow endothelial cells

BMECs were isolated according to a published protocol²⁰ with minor modifications. Briefly, femurs of 6- to 8-week-old DRM were dissected. Bone marrow cells were collected, filtered through a 70- μ m mesh, and plated in DMEM containing 15% FBS and penicillin/streptomycin at 20×10^6 /mL overnight. The non-adherent floating cells that contain BMECs were pelleted and cultured in a gelatin-coated plate containing complete EC growth medium overnight. The attached cells were vigorously washed, and the remaining adherent cells represented BMECs, passage 0. EC growth medium was refreshed every 3 days, and BMECs were split when they reached ~70% confluency.

Isolation of mouse lung endothelial cells

Lungs were collected from three 2- to 3-month-old DRM, placed in ice-cold PBS containing antibiotics, cut into very small pieces, and digested with 0.2% collagenase II. The digested cells were dispersed in a 16-gauge cannula, filtered through a 70- μ m mesh, and collected by centrifugation. Cells were cultured in a gelatin-coated plate in EC growth medium overnight. The attached cells represented mouse lung ECs (MLECs, passage 0). MLECs at passage 2 to 3 were used in *in vitro* studies.

In vitro tube formation of BMECs and MLECs

Tube formation assays were performed on growth factor-reduced Matrigel. Icy cold Matrigel was laid down on the bottom of wells in a 24-well plate in duplicate and solidified in a tissue culture incubator for 30 min. BMECs or MLECs were seeded on top of the Matrigel at 1×10^4 cells/well in 0.5 mL EC growth

medium. Tube formation was recorded for up to 24 h. BMECs and MLECs tube formation assays were performed two times and three times, respectively.

In vitro osteogenic differentiation assays for BMECs and MLECs

BMECs and MLECs were seeded in gelatin-coated 24-well culture plates at 1×10^5 cells/well with 0.5 mL EC growth medium. Upon confluence, cells were cultured in serum-free DMEM in the absence or presence of rhBMP4 (100 ng/mL)³ for 3 days followed by culturing in StemPro osteogenic differentiation medium in the absence or presence of rhBMP4 (100 ng/mL) for a minimum of 21 days, with medium refreshed twice per week. RFP and GFP fluorescence activities were monitored during the osteogenic differentiation period. At the end, cells were fixed in formalin and incubated with Alizarin Red S (ARS) solution for calcium deposit determination, and multiple images per well were quantified using ImageJ software. MLECs and BMECs *in vitro* osteogenic differentiation assays were performed four times and three times, respectively. Similarly, for osteogenic differentiation following *in vitro* tube formation assays, the vessels on Matrigel were cultured in serum-free DMEM in the absence or presence of rhBMP4 (100 ng/mL) for 3 days, followed by incubation in StemPro osteogenic differentiation medium in the absence or presence of rhBMP4 (100 ng/mL) for 17 days, with medium refreshed twice per week. RFP and GFP fluorescent activities were monitored during the differentiation period.

Isolation of CD31⁺ cells from MLECs and BMECs

Isolation of CD31⁺ subpopulations of BMECs and MLECs was performed using anti-mouse CD31 antibody-conjugated Dynabeads. Conjugation of anti-CD31 antibody to Dynabeads was prepared according to the manufacturer's protocol. For selection of CD31⁺ cells, BMECs and MLECs were incubated with CD31-Dynabeads for 30 min at room temperature, followed by the magnetic-binding selection. The selected cells were plated on gelatin-coated plates in EC growth medium for *in vitro* tube formation assays as well as *in vitro* osteogenic differentiation assays as described above.

FACS and RNAseq analysis

Femurs of three 2- to 3-month-old DRM were used to isolate RFP⁺ and RFP⁺/GFP⁺ cells from the bone marrow. Femurs with epiphyses removed were centrifuged to spin out the bone marrow cells. Cells were filtered through a 40- μ m mesh prior to FACS analysis. The sorted RFP⁺ and RFP⁺/GFP⁺ cells were used for RNAseq analysis. RNAs were prepared using the RNeasy kit (Qiagen) with DNase I treatments. RNAseq was performed at the Advanced Technology Genomics Core at MD Anderson Cancer Center. RNA fastq files were aligned to a *Mus musculus* genome assembly (version mm10 from Genome Reference Consortium GRCm38) using STAR (2.6.0b),⁶³ and raw counts were obtained using HTSeq.⁶⁴ Differentially expressed genes were identified using DeSeq2 with a false discovery cutoff of 0.05 and a fold-change cutoff of 2.⁶⁵ GSEAPreranked was used for GSEA^{66,67} as we only had two replicates.

GATA gene family analysis

To induce EC-to-OSB transition *in vitro*, MLECs and the 2H11 lymphoid EC line were cultured in serum-free DMEM overnight followed by treatment with BMP4 (100 ng/mL) in serum-free medium for 48 h as previously described.⁷ Total RNA was used for qRT-PCR analysis of GATA1–6 mRNAs using SYBR green fluorescence signals (Applied Biosystems). Knockdown of GATA3 by shRNA in 2H11-shGATA3 clones 6 and 7 was confirmed by qRT-PCR and Western blotting. Primer sequences used are listed in Table S2.

QUANTIFICATION AND STATISTICAL ANALYSIS

All quantitative results were expressed as mean \pm SD. The data was analyzed using two-sided Student's t-test. A value of $p < 0.05$ was considered to be statistically significant.